ACS Catalysis

Perspective

pubs.acs.org/acscatalysis

Metal Carbides as Alternative Electrocatalyst Supports

Ying Liu,[†] Thomas G. Kelly,[‡] Jingguang G. Chen,[§] and William E. Mustain*,[†]

[†]Department of Chemical and Biomolecular Engineering, University of Connecticut, 191 Auditorium Drive, Storrs, Connecticut 06269, United States

[‡]Department of Chemical and Biomolecular Engineering, University of Delaware, Newark, Delaware 19716, United States

[§]Department of Chemical Engineering, Columbia University, New York, New York 10027, United States

ABSTRACT: Transition metal carbides (TMCs) have attracted a significant amount of attention over the past few years as electrocatalyst support materials. TMCs are interesting because of their similar electronic structures to noble metals near the Fermi level (i.e., WC and Pt), which can promote electron transfer between the catalyst and its support—to enhance the stability of supported Pt nanoparticles as well as enhance its intrinsic activity for select reactions. This perspective article summarizes both theoretical and experimental results for Pt catalysts supported by TMCs for hydrogen evolution reaction (HER) and oxygen reduction reaction (ORR) to explore the interaction mechanism of the catalysts and the carbide supports. The strategies to improve the present carbide supports for HER and ORR are also discussed, which is expected to shed light on future development of TMC electrocatalyst supports.

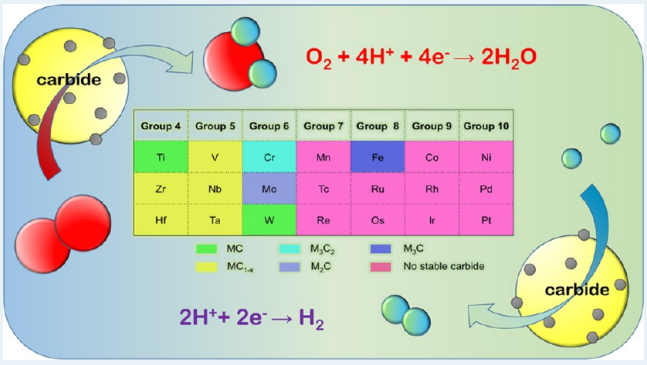

KEYWORDS: *carbide, catalyst support, DFT, hydrogen evolution reaction, oxygen reduction reaction*

1. INTRODUCTION

Transition metal carbides (TMCs) are an interesting class of materials as electrocatalyst supports since they are chemically stable in acidic media, resistant to poisoning, have excellent mechanical durability, and possess high electronic conductivity. For certain applications, they are more catalytically active or selective than their parent metals.[1,2] As catalyst supports, carbides form covalent-type bonds with deposited metals and effectively stabilize admetals.[3] The reduction of precious metal loading by using TMCs as supports offers a great opportunity for cost reduction in electrocatalytic applications.

The formation of carbides is extensive throughout the transition metals. Most transition metals, with the exception of Pt-group metals, form carbides. Additionally, the carbides of elements neighboring the Pt group metals are not stable, with the exception of Fe carbide. Table 1 shows the Group 4−10 metals and the stoichiometry of their most stable carbide.[4] Most stable carbides, such as TiC, VC, and NbC, exist in the B1 structure, which is an fcc lattice structure similar to NaCl. Others such as WC and Mo_2C have a hexagonal unit cell.[5] One much-noted feature is that the lattice adopted by the metal in the TMCs is never that of the parent metal. This has been explained using Engel−Brewer theory where the structure adopted by a metal or alloy depends on the number of sp electrons.[6] With increasing sp electrons the metal structure progresses from bcc to hcp to fcc. Likewise, the Group 4 and 5 metal carbides form in an fcc structure because the incompletely filled bands of the host metals can accommodate a high ratio of sp-electron-rich carbon. In Group 6, the stoichiometry M_2C occurs often, while for Group 7 and 8, the metal-rich stoichiometries M_3C and M_4C are preferred. These stoichiometries are a result of increased d-band filling in the metals.[7] Among them, the carbides of the transition metals in Groups 4−6 show chemical stability, degrading only by concentrated acid or base in the presence of oxidizing agents at room temperature and retaining good corrosion resistance at high temperatures.[8]

Table 1. Transition Metals of Groups 4−10 and Their Positions in the Periodic Table[4] (Produced from Data in Ref 4 2009, *Energies*)

Group 4	Group 5	Group 6	Group 7	Group 8	Group 9	Group 10
Ti	V	Cr	Mn	Fe	Co	Ni
Zr	Nb	Mo	Tc	Ru	Rh	Pd
Hf	Ta	W	Re	Os	Ir	Pt

MC, MC_{1-x}, M_3C_2, M_2C, M_3C, No stable carbide

Received: February 18, 2013
Revised: April 8, 2013
Published: April 24, 2013

   dx.doi.org/10.1021/cs4001249 | *ACS Catal.* 2013, 3, 1184−1194

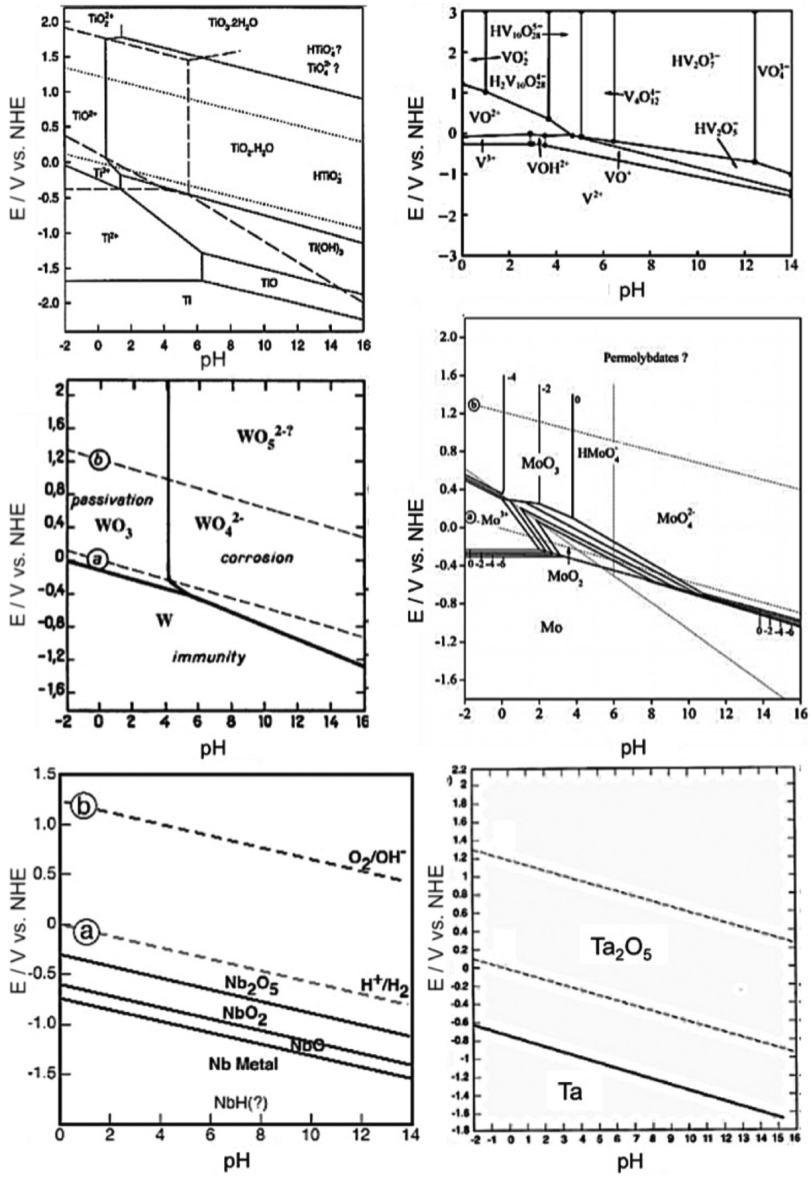

Figure 1. Pourbaix diagrams of the systems of metal-water, metal = (Ti, V, W, Mo, Nb, Ta), at 25 °C.[18] Produced using data from ref 18. Copyright 1966, Pergamon Press.

Unfortunately, these carbides are often difficult to prepare with high surface areas and free of contaminants. There have been a number of approaches to synthesize carbides with a high surface area, including carburization of a spray of the cprresponding oxide powder in a CH_4/H_2 gas mixture,[9] reaction of the metal oxide vapors with activated carbon,[10] and ultrasound irradiation of metal carbonyl compounds.[11] The problem of surface contamination has also been investigated, with most solutions focusing on the activation of the carbide surface via a thermal treatment prior to catalytic use. Thermal treatment can include heating in vacuum, which has been found to activate TaC, TiC, and WC for hydrogenation of ethylene,[12,13] or reducing in flowing hydrogen gas.[14] However, these methods only target the removal of surface oxygen. Recently, O_2 plasma treatment was applied to remove surface carbon on WC foil; this treatment successfully removed surface C while not affecting the carbide itself.[15]

In addition, the incorporation of carbon atoms significantly modifies the physical properties of Group 4−6 transition metals. This is likely due to the following effects, which induce electronic and structural changes that influence catalytic properties:[16] (1) The electronic interaction between the valence states of carbon and the parent metal, which can modify the density of states (DOS) of the metal near the Fermi level; (2) Tensile strain introduced by the incorporation of carbon, which typically increases the metal−metal distance and modifies the metal d-band; (3) The presence of carbon atoms on the surface reduces the number of metal sites available for the adsorption and reaction.

Although TMCs possess unique activity compared to their parent metals, their activity is not high enough for practical use as electrocatalysts. Alternatively, both theory and experiments show that they are promising candidates for catalyst supports.[4,17] In addition to activity, the stability of supported electrocatalysts is another important consideration and is determined by the following two effects: (1) stability of the supports and the noble metals in electrochemical environments, and (2) interaction between the carbide and the supported

dx.doi.org/10.1021/cs4001249 | ACS Catal. 2013, 3, 1184−1194

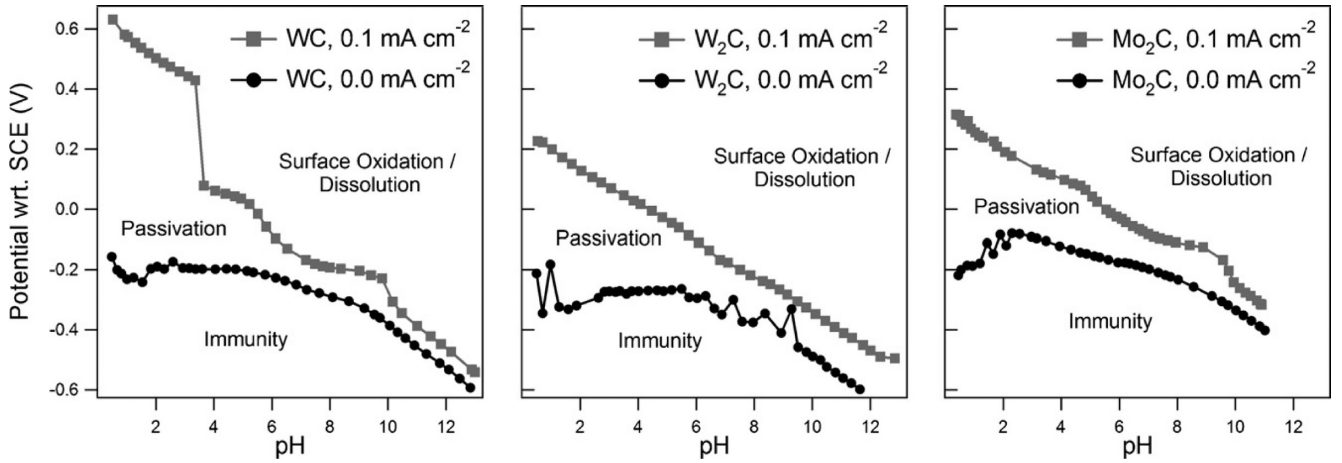

Figure 2. Stability maps of WC and Mo_2C. Samples were held at 0.0 mA cm^{-2} and 0.1 mA cm^{-2} to outline the regions of immunity, passivation, and surface oxidation/dissolution.[19] Reproduced with permission from ref 19. Copyright 2012, Elsevier.

metals. With regards to the first criterion, Pourbaix diagrams present the thermodynamically stable states of materials at different potential and pH values.[18] Although Pourbaix diagrams are typically only available for pure elements, the general stability of parent metals may extend to their carbide forms.

Figure 1 shows several Pourbaix diagrams of early transition metals at 25 °C in H_2O. All of the diagrams contain three distinct regions: (1) Immunity at negative potentials; (2) Passivation, wherein an insoluble oxide film can form, protecting the metal from further oxidation; (3) Corrosion, as the potentials increase further in some pH regions, metals and their oxides dissolve into solution. To maintain catalyst integrity, electrodes should only be operated in E-pH regions where immunity prevails. The early transition metals have the largest potential regions for immunity at reducing conditions and in acidic environments. It is likely that TMCs follow similar stability trends.

To study the electrochemical stability of carbides themselves, titration experiments have been conducted by Weidman et al.[19] Figure 2 shows the E-pH diagrams of WC, W_2C, and Mo_2C. The carbides showed similar trends in their E-pH stability, being immune at the same general conditions. Also, they exhibited large regions of passivation at low pH values and narrow passivation regions in neutral and alkaline solutions. One key difference was that WC exhibited a notably larger region of passivation in the pH range of 0.5−4.0. Thus, WC could be useful for applications whose operating conditions fall within this region. Comparing the stabilities of metallic tungsten and WC, it is obvious that they are similar. The only significant difference is that the surface oxidation/dissolution region of WC extends to a lower pH.

The electrochemical stability of other carbides has also been studied. For the case of TiC, Cowling and Hintermann[20] indicated that in 2 M H_2SO_4 solution, the initial corrosion of TiC produced TiO^{2+}, and at 0.91 V (all potentials are referred to NHE), the formation of passivating oxide began; as long as the potential was higher than 1.05 V, the rate of oxide formation exceeded the rate of its dissolution, and TiC became passivated. About 1.75 V, oxidation to TiO_2^{2+} occurred, and severe corrosion of the TiC followed. These corrosion behaviors are similar to those of metallic Ti, as shown in Figure 1. These results show that the Pourbaix diagrams of the transition metals can serve as a guide for TMC stability.

2. ELECTROCATALYSTS

On an electrochemical catalyst, the overall reaction usually consists of a series of elementary processes: adsorption/desorption, bond breaking and reorganization, and electron transfer. Though electron transfer and bond cleavage steps typically are rate limiting, adsorption strength and conformation play a critical role in defining the dominant reaction pathway. Qualitatively, the Sabatier principle[21] tells us that optimal catalytic activity can be achieved on a catalytic surface with "moderate" binding energies (or free energies of adsorption) for reactive intermediates.

One of the biggest challenges in catalysis is to establish a molecular-level understanding of reactions on the catalyst surface. Until recently, this insight was limited to physical experiments. With dramatic improvements in the performance of low-cost computing, researchers have utilized density functional theory (DFT) calculations to predict catalytic properties from first principles. These studies have improved our understanding of the relationship between catalyst properties and catalytic activity.[22,23]

With the development of DFT, the energy of a complex many-electron system can be determined as a function of the electron density. Using DFT, Norskov et al have correlated the electronic structure of metal surfaces to their catalytic activity in various systems.[24] Electronic structure is often described in terms of d-band center, which is the average energy of the d-band density of states. Since the d-band center of metal surfaces can be readily obtained by DFT calculations, it may be possible to predict catalytic activity by using the d-band center value as a descriptor.

For most metals, a single continuous energy band extends from low energy levels to high energy levels. The distribution of this energy band is normally called density of states (DOS). Figure 3 shows a scheme of a typical DOS for a transition metal, with broad s band and sharp d-band. To illustrate the surface adsorption process clearly, the DOS of Pt and O are shown for oxygen adsorption on the Pt(111) surface in Figure 4.[24] Consider that the O−Pt bond formation with the Pt surface s and d electrons takes place separately in two steps. In the first step, the valence O 2p state interacts with the s electrons of Pt and gives rise to a single resonance, which is well below the Fermi level and, hence, completely filled. Further coupling to the d electrons of the narrow d bands leads to

dx.doi.org/10.1021/cs4001249 | ACS Catal. 2013, 3, 1184−1194

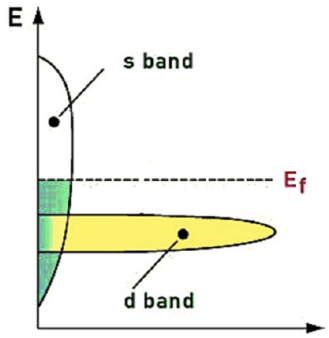

Figure 3. Schematic illustration of the DOS of a transition metal, showing the broad s band and the narrow d band around the Fermi level (E_f).[24] Reproduced with permission from ref 24. Copyright 2000, Elsevier.

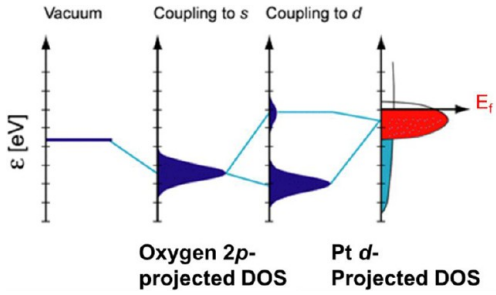

Figure 4. Schematic illustration of the change in local electronic structures of an oxygen atom adsorption on Pt surface.[24] Reproduced with permission from ref 24. Copyright 2000, Elsevier.

strong interaction and a splitting of the oxygen resonance into two states: a bonding state below Fermi level and fully filled; and an antibonding state that straddles the Fermi level and is thus partially filled.[25,26] For catalysts with different DOS, bond strength increases as the antibonding state decreases in electron density. Since the contribution from the interaction with metal sp states is approximately the same, the main trends in the adsorbate chemisorption energies can be determined by the interaction with the catalyst surface d electrons. As the d-band moves closer to the Fermi level, it becomes narrower. The antibonding orbitals formed by resonance are also narrower and thus, more likely to be located above the Fermi level. Thus, for the electrocatalytic reactions with the surface reactant adsorption as the rate-determining step, the surface d-band center (ε_d) is a strong descriptor for electrocatalyst activity.

3. HYDROGEN EVOLUTION REACTION

Over the years, the hydrogen evolution reaction (HER), which involves proton reduction and subsequent hydrogen evolution, has been found to be important for a variety of electrochemical processes. Technological interest in the HER is spread over applications as diverse as electrodeposition and corrosion of metals in acids and storage of energy via H_2 production. Pt is currently the most commonly implemented electrocatalyst for the HER. Although Pt is active for the HER, its high price remains a large barrier to electrolytic commercial hydrogen production. Several mechanisms have been proposed for polycrystalline Pt electrodes, and it is generally accepted that on polycrystalline Pt electrodes, between its formal potential and 0.4 V, hydrogen is strongly adsorbed onto the electrode surface by underpotential deposition until the surface concentration of H_{upd} is approximately a single monolayer. This reaction is shown in eq 1:

Volmer or discharge reaction:

$$H^+_{(aq)} + e^- \rightarrow H_{ad} \quad (1)$$

Then, there are two possible routes for the HER as the electrode potential passes through the formal potential:[27]

Tafel or combination reaction:

$$2H_{ad} \rightarrow H_{2,ad} \quad (2)$$

Heyrowsky or ion-atom reaction:

$$H_{ad} + H^+_{(aq)} + e^- \rightarrow H_{2,ad} \quad (3)$$

The Volmer reaction is usually considered to occur rapidly, leaving either the Tafel reaction or the Heyrowsky reaction as the rate-limiting step.

For constant activity of protons, fugacity of molecular hydrogen, and temperature, the electrocatalytic activity is crucially dependent on composition and surface structure of the catalysts. The HER activity is usually characterized by the exchange current density, i_0, which is proportional to the reaction rate for a given overpotential. Kinetic data for the HER were empirically found to correlate with its thermodynamic properties. Since the HER has one key reactive intermediate (adsorbed H), a relationship between HER activity and hydrogen binding energy (HBE) has been established.

When the catalytic activity of various metals for the HER is plotted as a function of the hydrogen−metal bond strength, a volcano-shaped plot is found,[28−30] in agreement with the Sabatier principle. The shape of such a volcano plot was rationalized independently by Parsons,[31] who deduced a model that i_0 was related to the standard free energy of hydrogen adsorption ΔG_H.[32,33] For very exergonic hydrogen adsorption ($\Delta G_H < 0$), the coverage of adsorbed hydrogen would be high, leading to steric hindrance and prevention of recombination to H_2.[32] For very endergonic adsorption ($\Delta G_H > 0$), a low driving force for H^+ adsorption would lead to low i_0.

For $\Delta G_{H^*} \approx 0$, these two regimes would be approximately balanced, and a maximum in the exchange-current density was predicted. This prediction was confirmed by Figure 5, which shows the experimentally measured HER exchange current densities against ΔG_H values calculated by DFT.[34] Although there is some scatter in the data, the figure clearly suggests that an optimum in the measured i_0 is found at ΔG_H values very close to zero.

Then, DFT was used to explore the theoretical relationship between the surface average d state energies (the local d-band center) of catalysts and their adsorption abilities for H_2. Greeley and Nørskov found that the local d-band center could predict the H adsorption energy and thus HER activity. As shown in Figure 6 for Pd-based bimetallic surfaces,[33] it is clear that the higher in energy the d states are, the stronger the bonds that are formed between adsorbed hydrogen atoms and the catalyst surface. The variations in electrocatalytic properties can therefore be correlated to variations in the electronic structure of the surface atoms. Thus, a volcano-type relationship between the catalyst surface d-band center and HER activities can be rationally expected. With the relationship between HER activity and electronic structure established for pure metals and alloys, recent research has examined these same properties for TMCs, which is discussed in the following paragraphs.

dx.doi.org/10.1021/cs4001249 | ACS Catal. 2013, 3, 1184−1194

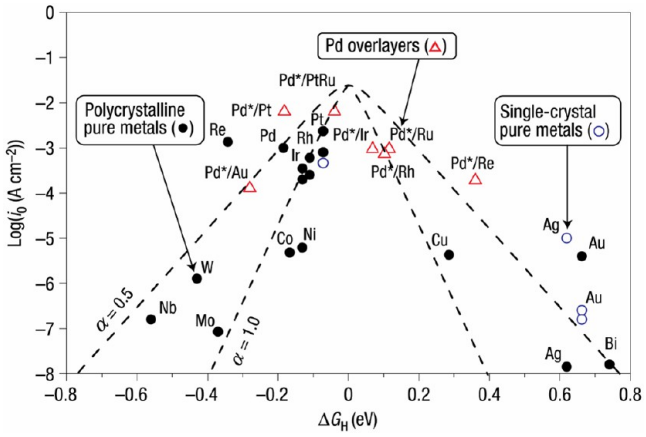

Figure 5. Volcano plot for the HER for various pure metals and metal overlayers, ΔG_H values are calculated at 1 bar of H_2 (298 K) and at a surface hydrogen coverage of either 1/4 or 1/3 ML. The two curved lines correspond to the activity predictions of simple mean-field, microkinetic models, assuming a transfer coefficient (α) of 0.5 and 1.0, respectively.[34] Reproduced with permission from ref 34. Copyright 2006, Nature Publishing Group.

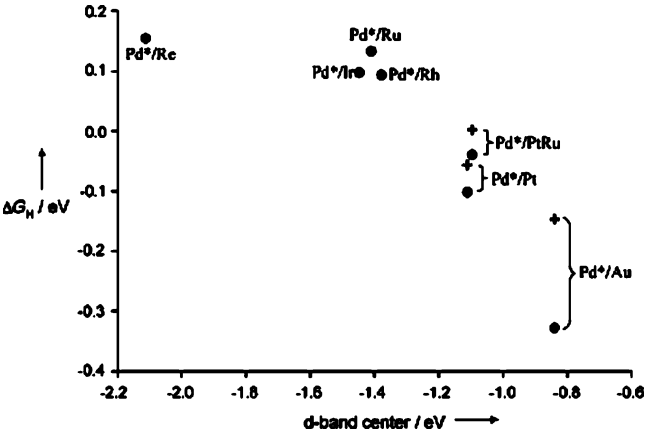

Figure 6. Differential free energy of hydrogen adsorption as a function of the clean surface d-band center. The black circles represent differential free energies at hydrogen coverage of 0.25 ML. The crosses represent differential free energies from 0.25 ML for only three systems.[33] Reproduced with permission from ref 33. Copyright 2006, John Wiley & Sons.

Wirth et al.[35]investigated the electrocatalytic performance of TMCs for HER in 0.1 M H_2SO_4. The performance of the TMCs was compared with transition metal nitrides, sulfides, silicides, and borides, with Pt and Ni as benchmarks. The HER overpotential has been a common way to describe activity. A three-dimensional plot of the overpotential as a function of transition metal and their refractory compounds is presented in Figure 7 to elucidate correlations between catalyst composition and performance. Tungsten has the highest activity among all the transition metals. Following is Mo, which is promising. The remaining transition metals may not possess sufficient HER activity to justify further research; When the refractory compounds are considered, the carbides represent the most promising group, followed by borides and silicides. By further comparing the HER activity of all the metals and compounds, shown in Figure 8 and summarized in Table 2, as expected and generally accepted, Pt has lowest overpotential and is followed by WC and Mo_2C at considerably increased overpotentials. At

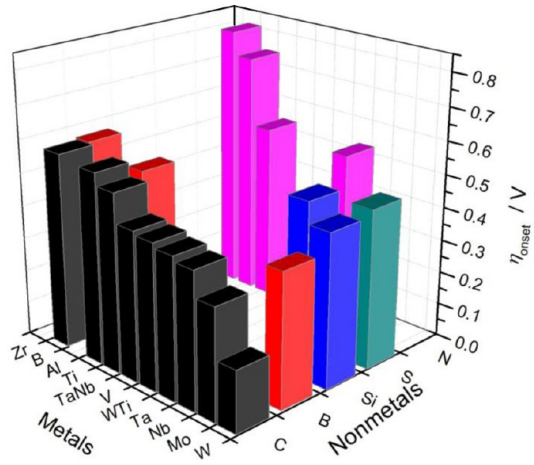

Figure 7. Three-dimensional plot of the overpotential for the hydrogen evolution reaction at the studied refractory ceramics as a function of their metal and nonmetal components. Low columns represent a high performance; high column represent low catalytic activity.[35] Reproduced with permission from ref 35. Copyright 2012, Elsevier.

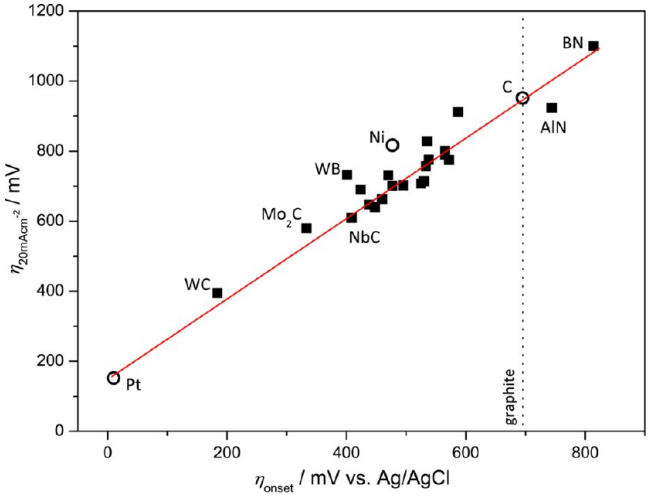

Figure 8. Correlation of the overpotential of the hydrogen evolution reaction at a current density of 20 mA cm^{-2} and the onset overpotential. The catalyst samples were mechanically immobilized at a graphite electrode and immersed in 0.1 M H_2SO_4. The scan rate was 5 mV s^{-1}, rotating at 1000 rpm.[35] Reproduced with permission from ref 35. Copyright 2012, Elsevier.

the opposite side, AlN and BN show higher overpotentials than bare carbon, which is not surprising considering their lack of d-electrons. This comprehensive study of transition metal compounds has elucidated general trends in HER activity, but has also reinforced the fact that these compounds are not active enough to be used as commercial HER electrocatalysts.

The stability of many TMCs have also studied in HER-relevant conditions, 0.1 M H_2SO_4 at an overpotential of −1 V as illustrated in Table 2. By comparing the corrosion rate, k_{corr}, of these carbides with the Pourbaix diagrams of their parent metals (Figure 1), it is found that the TMCs show a similar performance as their corresponding parent metals. Under the conditions of pH = 1 and E = −1 V, all the pure metals except Mo are in the immunity region of their Pourbaix diagrams. Correspondingly, NbC, TaC, and TiC show the lowest corrosion rate; VC should corrode severely since the condition

dx.doi.org/10.1021/cs4001249 | ACS Catal. 2013, 3, 1184−1194

Table 2. Detailed Analysis of the Overpotential Data and Corrosion Rates of the Carbide Eletrocatalysts for HER in a Constant Volume of 0.1 M H_2SO_4 and Polarized at a Constant Potential of −1 V[a] (Reproduced with Permission from Ref 35. Copyright 2012, Elsevier)

catalyst sample	E_{onset} /[mV] (vs Ag/AgCl)	η_{onset} /[mV]	$\eta_{20\_mA/cm2}$ /[mV]	k_{corr} /μmol d^{-1} cm^{-2}
Pt-Vulcan (20 wt %)	−240	10	201	0.36
Ni-powder	−707	477	866	
graphite powder	−925	695	1001	
B_4C	−817	587	961	13.94
Mo_2C	−563	333	629	152.81
NbC	−639	409	659	0.62
TaC	−654	424	739	0.36
TaNbC	−765	535	877	0.12
TiC	−802	572	824	1.56
VC	−678	448	689	24.02
WC	−414	184	444	5.64
WTiC	−668	438	696	1.2

[a]After about 15−20 h the metal concentration in the electrolyte was analyzed.[35]

(pH = 1 and −1 V) lies in the corrosion area of the Pourbaix diagram of its parent metal V. It should be noted that WC and Mo_2C both show corrosion rates, which seem to be in conflict with the pH-potential graphs proposed by Weidman et al. Mo_2C shows the highest corrosion rate. For WC the corrosion rate was found to be 5 $\mu mol_{catalyst}$ d^{-1} cm^{-2}, which is likely acceptable for commercial applications. However, the pH-potential graphs aimed to show regions of relative stability, not to accurately represent a true Pourbaix diagram. Even at the open-circuit potential, some corrosion will occur. Therefore, further quantitative research on the HER stability of WC and Mo_2C is needed.

HER Catalyst Supported on Tungsten Carbide. Esposito et al.[17] investigated the HER activity on transition metal, TMC, and Pt/TMC surfaces whose HBE values span a wide range of the HER volcano curve. In Figure 9, the i_0 values

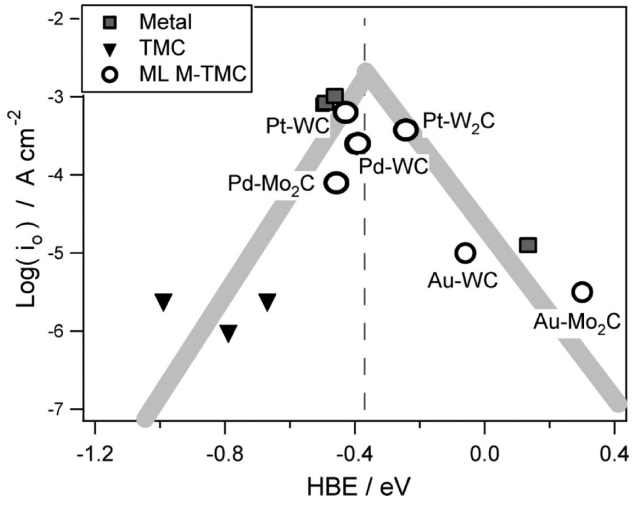

Figure 9. Volcano relationship between HER activity (i_0) and hydrogen binding energy (HBE) for all metal, TMC, and ML-metal-TMC thin film.[17] Reproduced with permission from ref 17. Copyright 2012, American Chemical Society.

determined from the Tafel plots for these surfaces are plotted versus the corresponding DFT-calculated HBE. These surfaces follow a volcano relationship like pure metals and bimetallics. As shown in Figure 9, the HBE for the unmodified WC surface is significantly greater than Pt, but that of 1 ML of Pt on WC is almost identical to that of bulk Pt. This suggests the possibility of supporting an active Pt surface on a bulk support of "platinum-like" WC. In the work of Liu and Mustain,[36] a monolayer of Pt nanoparticles were deposited on the surface of WC crystals, and evaluated as the electrocatalyst for the HER and HOR. It was found that Pt/WC showed improved activity compared with Pt/C and bulk Pt (Pt/WC showed a positive shift in both onset and half-wave potential), which was due to the high surface area of WC supports. Pt/WC was also more stable than Pt/C. Under identical operating conditions, Pt/WC lost only 4% of its activity, much less than the 20% lost by Pt/C. Most of the degradation of the Pt/WC performance was due to the dissolution of impurity WO_x species on the support surface from synthesis. In addition, the HER reaction kinetics for both Pt/WC and Pt/C were found to be identical, proceeding through the Volmer−Heyrovsky mechanism. These results further verify that Pt/WC can be used as a substitute for bulk Pt.

4. OXYGEN REDUCTION REACTION

The oxygen reduction reaction (ORR) is the rate-limiting reaction occurring at the cathode of proton exchange membrane fuel cells (PEMFC).[37] Over the past several years, the ORR has attracted considerable attention because of its slow kinetics. ORR electrocatalysts normally require high Pt loadings, which have made PEMFCs prohibitively expensive.[38,39] The need to decrease Pt loading in next-generation ORR electrocatalysts is of high importance, and increasing the mass activity of Pt is paramount to accomplishing that goal. The most popular approaches to achieving high Pt activity today include the use of supported catalysts and core−shell structures.

The ORR is a complex multistep reaction whose detailed mechanism is still debated today. Perhaps the most-commonly accepted ORR mechanism in acid solutions involves a combined adsorption/electron transfer step, followed by the breaking of the O−O bond shown in eq 4-7:

$$Pt + O_2 + e^- + H^+ \rightarrow Pt{-}OOH_{ads} \quad (4)$$

$$Pt - OOH_{ads} + Pt \rightarrow Pt{-}O_{ads} + PtOH_{ads} \quad (5)$$

$$Pt{-}O_{ads} + H^+ + e^- \rightarrow PtOH_{ads} \quad (6)$$

$$2PtOH_{ads} + 2H^+ + 2e^- \rightarrow 2Pt + 2H_2O \quad (7)$$

The overall four-electron reduction of O_2 is

$$O_2 + 4H^+ + 4e^- \rightarrow H_2O, \quad E^\circ = 1.23\ V \quad (8)$$

It is well-known that the ORR occurs mainly through either the direct or the parallel four-electron pathways on Pt-group metal catalysts. The rate-determining step is generally believed to be the first charge-transfer step, the O_2 adsorption with simultaneous charge and proton transfer to give an adsorbed Pt-OOH_{ads} species (eq 4). The adsorbed O and OH species then form because of the dissociation of the oxygen bond (eq 5), followed by the reduction of Pt−O_{ads} to Pt−OH_{ads} (eq 6). Further transfer of two electrons and two protons completes the four-electron reduction of O_2 to H_2O (eq 7). Irrespective of

dx.doi.org/10.1021/cs4001249 | ACS Catal. 2013, 3, 1184−1194

the microscopic mechanism, the ORR must involve the breaking of an O−O bond and the formation of O−H bonds. Thus, the ORR activity of an electrocatalyst is expected to correlate well to the surface oxygen binding energy (ΔE_0).

This speculation was confirmed by a kinetic model proposed by Norskov.[40] In this model, the activity of an electrocatalyst for the ORR is expressed as $k_BT \ln(r)$, where r is the rate per surface atom per second at an electrode potential of 0.9 V. Figure 10 shows how this model leads to a volcano-shaped

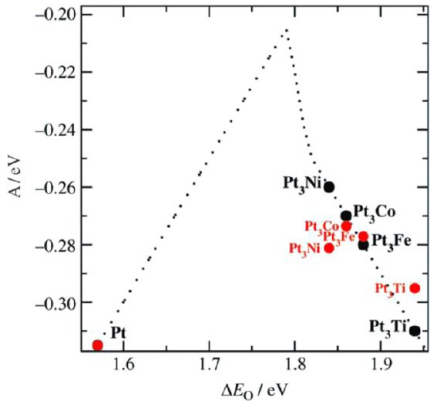

Figure 10. Model of the activity ($A = k_BT \ln(r)$, where r is the rate per surface atom per second) at an electrode potential of 0.9 V, as a function of the adsorption energy of oxygen, ΔE_0.[40] Reproduced with permission from ref 40. Copyright 2006, John Wiley & Sons.

dependence of the ORR rate on ΔE_0. For metals that bind oxygen too strongly (the maximum left), the rate is limited by the removal of adsorbed O and OH species, which limits the activity of Pt at elevated potentials. For metal surfaces that bind oxygen too weakly (the maximum right), the rate is limited by the electron transfer and subsequent dissociation of O_2. As discussed above, surface binding energies correlate with the d-band center. This conclusion also holds for the binding of oxygen;[40,41] Figure 11 shows the linear relationship between the oxygen binding energy and d-band center for Pt and Pd alloy systems. As discussed above, the position of ε_d for metal overlayers is affected by strain, coordination, and the electronic coupling between the overlayers and their substrate. It was also shown that the compressive strain tends to downshift ε_d in energy, causing adsorbates to bind less strongly, whereas tensile strain has the opposite effect. Some interpretations of the properties of the overlayer metals involve shifts of core levels because of a charge transfer between the overlayer and the substrate, or changes in the DOS near the Fermi level. Furthermore, it is believed that a slight increase in the 5d vacancy of Pt, resulting from its electronic interaction with the substrate, can increase the binding energy of O_2, thereby enhancing its catalytic activity toward the ORR. Thus, by introducing TMCs as supports for Pt group metals, the d band center of Pt may be shifted to the desired point. Additionally, TMCs may stabilize Pt overlayers during reaction.

ORR Catalyst Supported on Tungsten Carbide. W_2C microspheres were investigated as Pt supports by Ganesan.[42] Using cyclic voltammetry in acidic solutions, the electrochemically active area (ECA) of Pt supported on W_2C was found to be several times higher than Pt supported on either carbon microspheres or commercial carbon at identical loading. This result suggested that Pt particles could be better dispersed on W_2C. However, Zellner[43] showed that the W_2C phase was electrochemically unstable at potentials higher than 0.4 V, too low of a potential for an ORR electrocatalyst. For tungsten monocarbide, Hsu et al.[44] calculated oxygen binding energy on Pt (111), WC (0001), and one monolayer of Pt on WC (0001) (Table 3). The oxygen binding energy on WC was almost twice

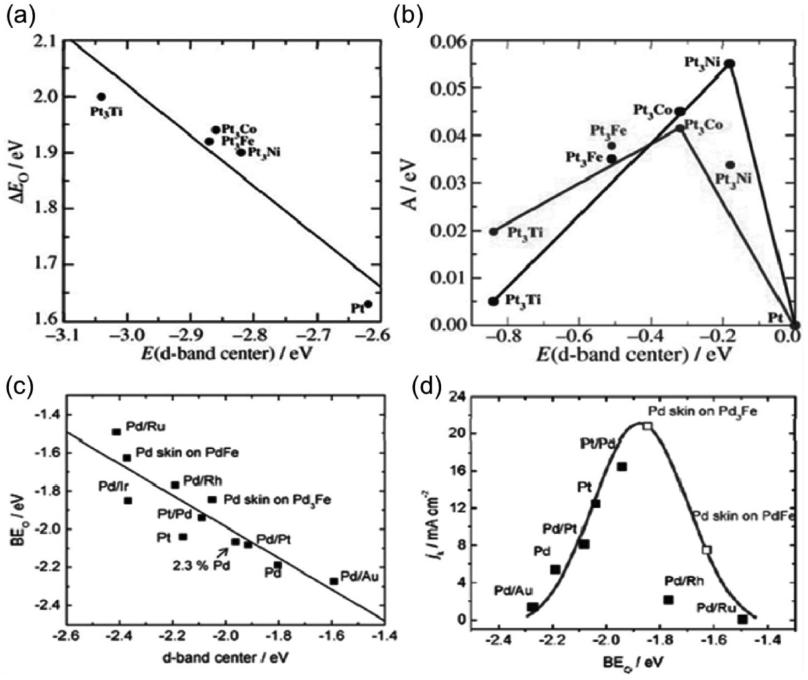

Figure 11. Linear relationship between the d-band center and oxygen binding energies (a) (c) and the resulting volcano-type behavior for ORR activity (b) (d) reported for Pt by Norskov[40] and Pd by Adzic.[41] Reproduced with permission from ref 40, copyright 2006, John Wiley & Sons, and from ref 41, copyright 2007, American Chemical Society.

dx.doi.org/10.1021/cs4001249 | ACS Catal. 2013, 3, 1184−1194

Table 3. Oxygen Binding Energies of Pt, WC, and 1 ML Pt on WC using 1/9 ML Coverage of Atomic Oxygen[44] (Reproduced with Permission from Ref 44. Copyright 2011, American Chemical Society)

surface	oxygen binding energy (kcal/mol)
Pt (111)	91.7
1 ML Pt on WC (0001)	92.9
WC (0001)	173.2

as high as on Pt. However, the binding energy changed considerably once one monolayer of Pt was added, and the value was close to that of Pt (111). This similarity suggests that a monolayer of Pt on WC could be as effective of an ORR catalyst as bulk Pt.

Liu and Mustain[36] also investigated Pt/WC electrocatalysts for the ORR. In this study, 3 nm Pt nanoparticles were well-dispersed on high surface-area WC crystals. During polarization, a significant positive shift in the ORR half-wave potential was observed for Pt/WC as compared to Pt/C, which showed a likely synergistic effect between Pt and WC. However, after 300 cycles between 0.2 and 1.0 V, the activity enhancement of Pt/WC was lost. In post-mortem analysis, it was found that surface WC could be oxidized to WO_x at potentials >0.8 V. This oxide formation led to two different Pt surface morphologies (Figure 12). The first group of Pt

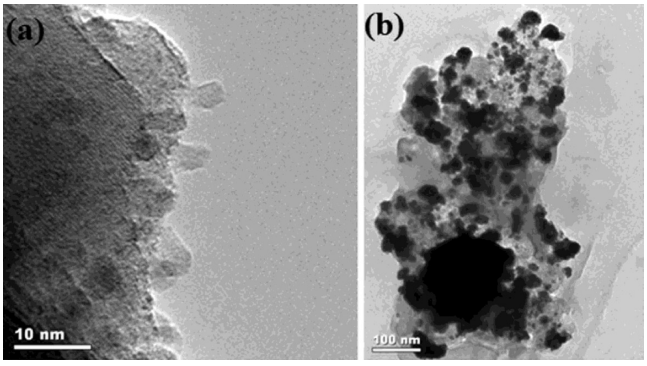

Figure 12. Platinum clusters deposited on WC supports before (a) and after (b) electrochemical experiments, showing the poor stability of the Pt particles due to WO_x formation.[36] Reproduced with permission from ref 36. Copyright 2011, American Chemical Society.

particles were still strongly bonded to the support surface with an average size of 3 nm. The second were 50−200 nm Pt clusters, which formed by detached Pt nanoparticles. Since WO_x was further converted to the water-soluble hydrogen tungsten bronze (H_xWO_3), Pt nanoparticles detached into solution with H_xWO_3 dissolution.

Yin et al.[45] investigated PdFe-WC electrocatalysts supported on carbon for ORR. PdFe catalysts had previously been shown to be active for ORR and tolerant to alcohol,[46,47] which could address one of the primary limitations of direct alcohol PEM fuel cells. ORR experiments found that despite the lower intrinsic activity of PdFe-WC/C catalysts compared to PdFe/C and Pt/C, the activity loss in the presence of methanol was minimal. However, because of the WC severe oxidation at high potentials, the stability of the PdFe-WC/C still needs to be improved. The degradation of the WC crystals at ORR-relevant potentials suggests that WC can be a useful Pt support only if its oxidation potential can be pushed to higher values or if alternative geometries can be realized.[48]

ORR Catalyst Supported on Molybdenum Carbide. Molybdenum carbide has also been shown to be a highly active catalyst for several chemical reactions. Previously, investigators believed that the platinum-like catalytic properties of Mo_2C were due to a change in the number of d-electrons. By adding the four valence electrons of carbon to the Mo valence electrons, the d-electron count of Mo could increase to be almost identical to the d-electron count of Pt. However, it was shown by Liu et al.[49] that for γ-Mo_2C (001) there was a strong coupling between d orbitals of Mo and sp orbitals of carbon, leading to a broadening of the surface Mo d band, thus a downshift of the d-band center of Mo. Then, Kitchin[50] found that the number of the d-electrons on both Mo- and C-terminated β-Mo_2C (0001) carbide surfaces were nearly the same as that of the Mo(110) surface, which suggests that carbon atoms do not donate their electrons to the Mo (Table 4) and the reason for the high activity of Mo_2C was not the

Table 4. Calculated Number of d-Electrons/Surface Mo Atom in Mo (110) and β-Mo_2C (0001)[50] (Reproduced with Permission from Ref 50. Copyright 2005, Elsevier)

surface	d-electrons/surface metal atom
Mo (110)	6.47
Mo-terminated β-Mo_2C (0001)	6.45
C-terminated β-Mo_2C (0001)	6.69
Pt (111)	9.26

electron donation. These differing conclusions could be the result of different Mo_2C structures and theoretical calculation methods. Hydrogen adsorbs more weakly to some sites of β-Mo_2C (0001) than to Mo (110) on carbon-terminated surfaces, which suggests that surface C-atoms are passivating. However, considering that early transition metals tend to bind too strongly to be efficient catalysts, if used as the catalysts by themselves, the carbon-terminated carbide surfaces should be preferred.

Pang et al.[51] used a microwave assisted thermolytic route to prepare nanostructured Mo_2C/CNTs composites, which was platinized through a polyol process. Pt/CNT samples with identical Pt loading (20 wt %) were also prepared. TEM images show the well-dispersed 5 nm Pt particles on Mo_2C/CNTs (Figure 13). Electrochemical results also indicated that the Pt/Mo_2C/CNT catalyst has higher ECA and a lower ORR

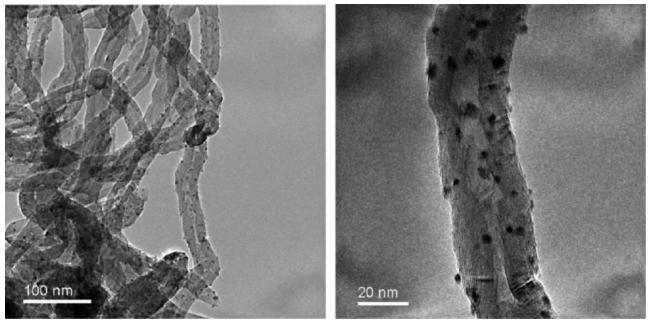

Figure 13. TEM images unplatinized (left) and platinized (right) Mo_2C/CNT catalysts that show homogeneous structure and well, dispersed supported Pt nanoparticles.[51] Reproduced with permission from ref 51. Copyright 2010, American Chemical Society.

dx.doi.org/10.1021/cs4001249 | ACS Catal. 2013, 3, 1184−1194

overpotential compared with Pt/CNT. Though the result was promising, the authors did not report the effects of potential cycling on support stability, which was a limiting factor with WC supports. Since Mo_2C oxidizes at a much lower potential than WC, it is expected that Pt/Mo_2C would have limited electrochemical stability at ORR-relevant potentials.

ORR Catalyst Supported on Titanium Carbide. Titanium carbide (TiC) has attracted interest because of its superior corrosion resistance.[52] LaConti et al.[53] found that at potentials higher than 0.8 V, TiC-based bipolar plates were more stable than carbon or graphite materials in various acids. In addition, TiC also improved the activity of the catalysts as the supports. Jalan et al.[54] found that Pt/TiC showed ORR activity six times higher than conventional Pt/C at 200 °C in 100% H_3PO_4. However, Ignaszak et al.[52] reported that TiC undergoes irreversible electrochemical oxidation in dilute $HClO_4$ above 0 V. To improve stability, the authors prepared TiC particles with a protective oxide layer, core−shell TiC@TiO_2 composites. It was found that the supported catalyst Pt_3Pd/TiC@TiO_2 showed much better ORR stability (45% mass activity loss after 500 cycles) than that of the Pt_3Pd/TiC (almost 100% mass activity loss after 500 cycles); thus this TiC@TiO2 core−shell structure is promising for the future research.

ORR Catalyst Supported on Vanadium Carbide. Hu et al.[55] reported the synthesis of cubic vanadium carbides uniformly dispersed on a carbon matrix by a hydrothermal method. The Pt nanoparticles were dispersed on both the carbon support and VC. The mass activity of ORR at 0.9 V was found to be 230 mA/mg_{Pt} for this catalyst, which was 2.4 times larger than that of commercial Pt/C (20 wt % Pt, 97 mA/mg_{Pt}). The authors suggested that the enhanced activity was due to a synergistic effect between Pt and VC, though the nature of this interaction was not discussed. And the results of stability experiments were not reported.

ORR Catalyst Supported on Iron Carbide. DFT was used to predict the activity and stability of a shell-anchor-core (Pt−Fe_2C−Ir) ORR electrocatalyst (Figure 14). In this case, two subsurface layers of Fe were replaced with Fe_2C,[56] which resulted in improved oxygen reduction activity in parallel to enhanced resistance against dissolution. The improved ORR activity was attributed mainly to reduced strain introduced by the subsurface Fe_2C compared with Fe, since the presence of C could reduce the lattice mismatch between the Fe and Pt elements. Lower strain led to a more moderate oxygen binding energy. In addition, the C atoms locked the transition metal atoms in their positions, preventing their segregation toward the surface. Without Fe diffusion to the surface, metals were prevented from dissolving into solution, which would lead to good long-term stability if synthesized.

ORR Catalyst Supported on Bimetallic Carbide. Researchers have explored new ways to stabilize the carbide materials under ORR conditions. One such method is to synthesize bimetallic carbide nanocomposites. Ma et al.[57] prepared nanocomposites consisting of the bimetallic carbide $Co_6Mo_6C_2$ supported on graphitic carbon by an anion-exchange method. Pt nanoparticles were loaded onto the catalyst, and it was evaluated for the ORR in 0.1 M $HClO_4$. The Pt/$Co_6Mo_6C_2$/C catalyst showed superior activity and stability in comparison with commercial Pt/C, as shown in Figure 15. The high performance was explained by a synergistic effect between the $Co_6Mo_6C_2$ support and Pt, which was due to the electron-donation of $Co_6Mo_6C_2$ and resulted in a change of Pt surface electronic structure. The catalyst was also stable after 1,000 potential cycles between 0.05 and 1.1 V as seen in Figure 15.

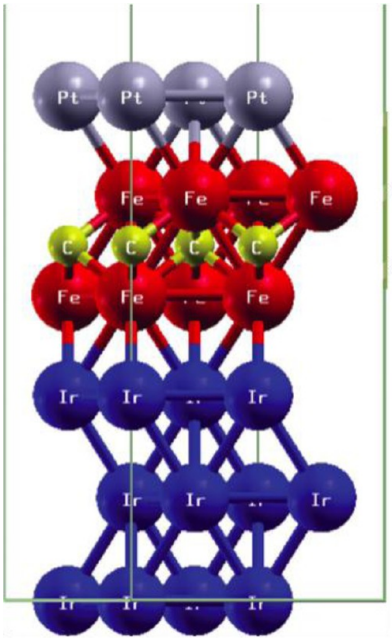

Figure 14. Slab model of the shell-anchor-core surface of Pt−Fe_2C−Ir.[56] Reproduced with permission from ref 56. Copyright 2010, AIP.

Generally, the ORR activity of low-cost carbide supported electrocatalysts can surpass that of electrocatalysts with carbon supports. The enhancement seems to correlate with the change of the Pt surface d-band center, which mainly results from the strain introduced by carbide supports and electronic interaction between the carbide and Pt particles. Especially, WC shows the ability to replace bulk Pt, and the activity of Pt/WC may be further enhanced by elimination of excess surface carbon and minimization of the Pt particle size to maximize the surface strain and active sites. WC and Mo_2C have the potential to be promising supports for Pt if their stability could be improved at high potentials. The bimetallic carbide $Co_6Mo_6C_2$ has high ORR activity and an exceptional stability against Pt dissolution under potential cycling. Further research can focus on enhancing the stability of carbides such as WC and the development of various bimetallic carbides.

5. CONCLUSIONS AND FUTURE OPPORTUNITIES

The current perspective leads to several areas for future work: (1) DFT calculations and electron spectroscopic measurements can help understand how the metal-carbide interaction affects the electronic properties of metal-modified carbides. Such a property-activity relationship will lead to the prediction of desirable metal-modified carbides for specific catalytic or electrocatalytic reactions; for example, the volcano shaped-curve for ORR and HER. (2) Supporting precious metal on WC and Mo_2C shows promise in significantly reducing the precious metal usage in electrocatalysts, in particular for ORR and HER. However, theoretical predictions are not always consistent with experimental results. The reason may be that the catalyst activity is decided by both the electronic and the geometric structures of the catalyst surface. Electrocatalysts with different sizes, shapes, facets, or surface impurities can lead to a variety of activities for the same material. In addition,

dx.doi.org/10.1021/cs4001249 | ACS Catal. 2013, 3, 1184−1194

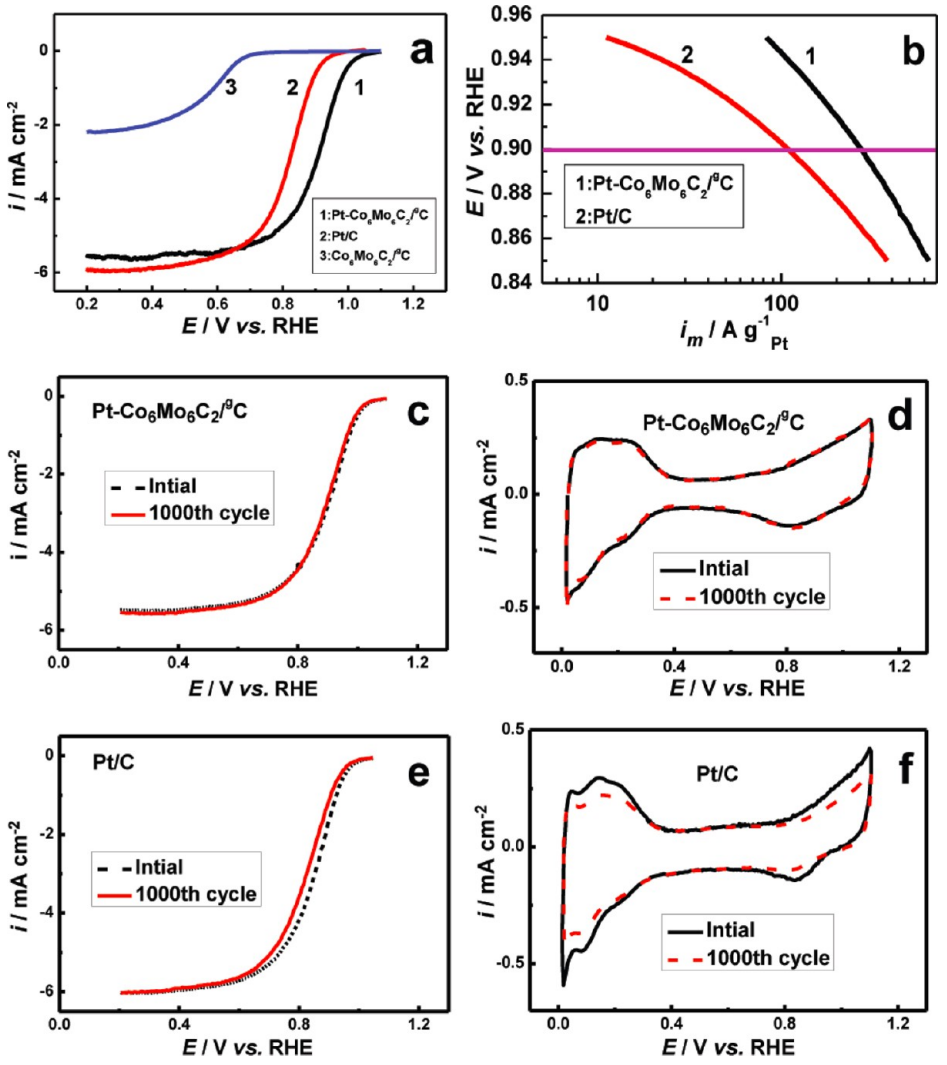

Figure 15. (a) Linear potential sweep curves for the ORR on Pt/C, $Co_6Mo_6C_2$/gC and Pt-$Co_6Mo_6C_2$/gC. (b) Mass activities for the ORR on two different catalysts. (c, e) ORR curves before and after 1000 cycles on (c) Pt-$Co_6Mo_6C_2$/gC and (e) Pt/C catalysts. (d, f) CVs before and after 1000 cycles on (d) Pt-$Co_6Mo_6C_2$/gC and (f) Pt/C in background solution.[57] Reproduced with permission from ref 57. Copyright 2012, American Chemical Society.

theoretical calculations tend to be based on ideal surfaces, which are almost never realized in real catalysts. Thus, systematic experimental studies with different sizes, shapes and facets are needed to understand the intrinsic activities of these electrocatalysts. (3) More detailed efforts are needed understand the long-term stability of carbide-supported electrocatalysts for different applications. Of particular interest is discovering new geometries, passivating layer, and additives (i.e., mixed metal carbides) that expand the immunity of carbide supports to higher potentials in acidic media, particularly for WC and Mo_2C.

AUTHOR INFORMATION

Corresponding Author

*E-mail: mustain@engr.uconn.edu.

Notes

The authors declare no competing financial interest.

REFERENCES

(1) Christian, J. B.; Smith, S. P. E.; Whittingham, M. S.; Abruña, H. D. *Electrochem. Commun.* **2007**, *9*, 2128−2132.
(2) Levy, R. B.; Boudart, M. *Science* **1973**, *181*, 547−549.
(3) Kharlamov, A. I.; Kirillova, N. V. *Powder Metall. Met. Ceram.* **1983**, *22*, 123−134.
(4) Ham, D.; Lee, J. *Energies* **2009**, *2*, 873−899.
(5) Oyama, S. T. *Catal. Today* **1992**, *15*, 179−200.
(6) Brewer, L. *Science* **1968**, *161*, 115−122.
(7) Ted Oyama, S. *J. Solid State Chem.* **1992**, *96*, 442−445.
(8) Silvestroni, L.; Sciti, D. *Adv. Mater. Sci. Eng.* **2010**, *2010*, 11.
(9) Lee, J. S.; Oyama, S. T.; Boudart, M. *J. Catal.* **1987**, *106*, 125−133.
(10) Ledoux, M. J.; Huu, C. P.; Guille, J.; Dunlop, H. *J. Catal.* **1992**, *134*, 383−398.
(11) Suslick, K. S.; Hyeon, T.; Fang, M.; Cichowlas, A. A. *Mater. Sci. Eng., A* **1995**, *204*, 186−192.
(12) Vidick, B.; Lemaître, J.; Leclercq, L. *J. Catal.* **1986**, *99*, 439−448.
(13) Kojima, I.; Miyazaki, E.; Inoue, Y.; Yasumori, I. *J. Catal.* **1982**, *73*, 128−135.
(14) Ledoux, M. J. G., J. L.; Pham-Huu, C.; Maria, S. U.S. Patent 5 139 987, 1992.
(15) Yang, X.; Kimmel, Y. C.; Fu, J.; Koel, B. E.; Chen, J. G. *ACS Catal.* **2012**, *2*, 765−769.
(16) Chen, J. G. *Chem. Rev.* **1996**, *96*, 1477−1498.
(17) Esposito, D. V.; Hunt, S. T.; Kimmel, Y. C.; Chen, J. G. *J. Am. Chem. Soc.* **2012**, *134*, 3025−3033.

(18) Pourbaix, M. *Atlas of Electrochemical Equilibria in Aqueous Solutions*; Pergamon Press: Oxford, U.K., 1966.
(19) Weidman, M. C.; Esposito, D. V.; Hsu, Y.-C.; Chen, J. G. *J. Power Sources* **2012**, *202*, 11−17.
(20) Cowling, R. D.; Hintermann, H. E. *J. Electrochem. Soc.* **1970**, *117*, 1447−1449.
(21) Sabatier, P. *Ber. Dtsch. Chem. Ges.* **1911**, *44*, 1984−2001.
(22) Nilsson, A.; Pettersson, L. G. M. *Surf. Sci. Rep.* **2004**, *55*, 49−167.
(23) Gajdoš, M.; Eichler, A.; Hafner, J. *J. Phys. Cond. Mat.* **2004**, *16*, 1141−1164.
(24) Hammer, B.; Nørskov, J. K. In *Advances in Catalysis*; Bruce, C., Gates, H. K., Eds.; Academic Press: New York, 2000; Vol. *45*, pp 71−129.
(25) Brown, W. A.; Kose, R.; King, D. A. *Chem. Rev.* **1998**, *98*, 797−832.
(26) Lundqvist, B. I.; Gunnarsson, O.; Hjelmberg, H.; Nørskov, J. K. *Surf. Sci.* **1979**, *89*, 196−225.
(27) Breiter, M. W. *Handbook of Fuel Cells: Fundamentals, Technology and Applications*; Wiley: Chichester, U.K.,2003; pp 361 −367.
(28) Conway, B. E.; Bockris, J. O. M. *J. Chem. Phys.* **1957**, *26*, 532−541.
(29) Trasatti, S. *J. Electroanal. Chem. Interfacial Electrochem.* **1972**, *39*, 163−184.
(30) Gerischer, H. *Bull. Soc. Chim. Belg.* **1958**, *67*, 506.
(31) Parsons, R. *Trans. Faraday Soc.* **1958**, *54*, 1053−1063.
(32) Nørskov, J. K.; Bligaard, T.; Logadottir, A.; Kitchin, J. R.; Chen, J. G.; Pandelov, S.; Stimming, U. *J. Electrochem. Soc.* **2005**, *152*, J23−J26.
(33) Greeley, J.; Nørskov, J. K.; Kibler, L. A.; El-Aziz, A. M.; Kolb, D. M. *ChemPhysChem* **2006**, *7*, 1032−1035.
(34) Greeley, J.; Jaramillo, T. F.; Bonde, J.; Chorkendorff, I.; Norskov, J. K. *Nat. Mater.* **2006**, *5*, 909−913.
(35) Wirth, S.; Harnisch, F.; Weinmann, M.; Schröder, U. *Appl. Catal., B* **2012**, *126*, 225−230.
(36) Liu, Y.; Mustain, W. E. *ACS Catal.* **2011**, *1*, 212−220.
(37) Santos, L.; Freitas, K.; Ticianelli, E. *J. Solid State Electrochem.* **2007**, *11*, 1541−1548.
(38) Meng, H.; Shen, P. K. *J. Phys. Chem. B* **2005**, *109*, 22705−22709.
(39) Meng, H.; Shen, P. K. *Chem. Commun.* **2005**, 4408−4410.
(40) Stamenkovic, V.; Mun, B. S.; Mayrhofer, K. J. J.; Ross, P. N.; Markovic, N. M.; Rossmeisl, J.; Greeley, J.; Nørskov, J. K. *Angew. Chem.* **2006**, *118*, 2963−2967.
(41) Shao, M.; Liu, P.; Zhang, J.; Adzic, R. *J. Phys. Chem. B* **2007**, *111*, 6772−6775.
(42) Ganesan, R.; Lee, J. S. *Angew. Chem., Int. Ed.* **2005**, *44*, 6557−6560.
(43) Zellner, M. B.; Chen, J. G. *Catal. Today* **2005**, *99*, 299−307.
(44) Hsu, I. J.; Hansgen, D. A.; McCandless, B. E.; Willis, B. G.; Chen, J. G. *J. Phys. Chem. C* **2011**, *115*, 3709−3715.
(45) Yin, S.; Cai, M.; Wang, C.; Shen, P. K. *Energy Environ. Sci.* **2011**, *4*, 558−563.
(46) Guczi, L. *Catal. Today* **2005**, *101*, 53−64.
(47) Li, W.; Haldar, P. *Electrochem. Commun.* **2009**, *11*, 1195−1198.
(48) Hsu, I. J.; Kimmel, Y. C.; Jiang, X.; Willis, B. G.; Chen, J. G. *Chem. Commun.* **2012**, *48*, 1063−1065.
(49) Liu, P.; Rodriguez, J. A. *Catal. Lett.* **2003**, *91*, 247−252.
(50) Kitchin, J. R.; Nørskov, J. K.; Barteau, M. A.; Chen, J. G. *Catal. Today* **2005**, *105*, 66−73.
(51) Pang, M.; Li, C.; Ding, L.; Zhang, J.; Su, D.; Li, W.; Liang, C. *Ind. Eng. Chem. Res.* **2010**, *49*, 4169−4174.
(52) Ignaszak, A.; Song, C.; Zhu, W.; Zhang, J.; Bauer, A.; Baker, R.; Neburchilov, V.; Ye, S.; Campbell, S. *Electrochim. Acta* **2012**, *69*, 397−405.
(53) LaConti, A. B. G., A. E.; Cropley, C. C.; Kosek, J. A. U.S. Patent 6 083 641, 2000.
(54) Jalan, V.; Frost, D. G. U.S. Patent 4 795 684,1989.
(55) Hu, Z.; Chen, C.; Meng, H.; Wang, R.; Shen, P. K.; Fu, H. *Electrochem. Commun.* **2011**, *13*, 763−765.
(56) Ramirez-Caballero, G. E.; Hirunsit, P.; Balbuena, P. B. *J. Chem. Phys.* **2010**, *133*, 134705.
(57) Ma, X.; Meng, H.; Cai, M.; Shen, P. K. *J. Am. Chem. Soc.* **2012**, *134*, 1954−1957.